J Mater Sci: Mater Electron (2016) 27:10252–10258
DOI 10.1007/s10854-016-5105-1

Effects of thickness and deposition temperature of ALD ZnO on the performance of inverted polymer solar cells

Ming Fang[1] · Lei Qi[1] · Chunmei Zhang[1] · Qiang Chen[1]

Received: 4 January 2016 / Accepted: 30 May 2016 / Published online: 2 June 2016

Abstract In this paper, we fabricated atomic layer deposition (ALD) ZnO films to modify indium tin oxide (ITO) electrode for the purpose of the efficient and stable inverted polymer solar cells (PSCs). The role of thickness and the deposition temperature of ZnO layer on the performance of the device was investigated. The results showed that more than 10 nm of ALD ZnO film was required to improve the photovoltaic performance of PSCs. When the deposition temperatures of the ZnO films were varied from 60, 110 to 190 °C, the chemical compositions, the crystal orientations and the mobility of the ZnO films were quite different, while, the work functions of modified ITOs were similar. It was found that the ZnO film could reduce the work function of ITO and turn it into an electron-collecting electrode. The performances of inverted polymer solar cells with the ZnO films deposited at different temperature were identical. We then concluded that the work function of thin ZnO played a crucial role when nano-thickness of ALD ZnO was used as the electron transport layer. As a result, the ALD ZnO films showed a promising interface layer for achieving air-stable plastic cells with roll-to-roll mass production potential.

Electronic supplementary material The online version of this article (doi:10.1007/s10854-016-5105-1) contains supplementary material, which is available to authorized users.

✉ Chunmei Zhang
zhangchunmei@bigc.edu.cn

[1] Laboratory of Plasma Physics and Materials, Beijing Institute of Graphic Communication, 102600 Beijing, China

1 Introduction

Polymer solar cells (PSCs) are rapidly developing due to its substantial advantages such as flexible substrates, light weight, large area fabrication process and low-cost potential [1–4]. Recently the main works are focusing on the efficiency improvement, the stability and energy conversion mechanism of PSCs. Although the power conversion efficiencies of conventional PSCs have reached 10 %, the poor stability has always prevented its applications [5–8]. The low work function metal anode such as aluminum or calcium is easily oxidized when it is exposed to air. Besides, indium tin oxide (ITO) can be corroded by poly(3,4 ethylenedioxylenethiophene): poly(styrene sulfonic acid) (PEDOT: PSS), and results in the decrease of the device performance [9–12]. Inverted PSCs overcome these shortcomings because of the use of the high work function metal as the top hole-collecting electrode [10, 11, 13–15]. However, the ITO as a cathode electrode does not demonstrate a good electron collection capability due to the energy level mismatch between the cathode and the LUMO of the acceptor in the active layer. Therefore, the surface modification of ITO with an electron transport layer was performed by the materials such as PEO [16], Al_2O_3 [17], Cs_2CO_3 [18, 19], TiO_2 [20, 21], ZnO [22–25] to adjust the work function. In these materials, the ZnO has been widely used because of its high electron mobility and the suitable energy level [22, 26]. Atomic layer deposition (ALD) method, based on the self-limiting characteristic of the reaction between reactant gas and solid surface, can deposit the uniform, dense, pinhole-free ZnO films at low temperatures [27]. And this method can also control the thickness of the films accurately by varying the number of the deposition cycles. Therefore, ALD is suitable for the fabrication of metal oxide films as electron transport layer

in polymer solar cells. [28]. In this work, we used ALD technique to deposit ZnO films as electron transport layer in inverted PSCs, and investigated the influence of the thickness and deposition temperature on the characteristic of ZnO films and the performance of the devices.

2 Experimental

Patterned ITO glass substrates (120 nm thickness of ITO glass with a sheet resistance of 15 Ω/sq) were cleaned in an ultrasonic bath with detergent, alcohol, acetone and de-ionized water sequentially for 10 min, respectively. Then the substrates were dried by N_2 stream and exposed to ultraviolet light for 5 min. The ZnO thin films were deposited on the cleaned ITO substrates by ALD, using diethyl zinc (DEZ) and water as the precursors. The pulse times of the precursors of DEZ and water were both set as 0.1 s, and the N_2 purging times (100 sccm) were set as 30 s and 60 s for DEZ and water, respectively. When we varied the thickness of the ZnO film, all the films were deposited at 110 °C and the deposition cycle of ZnO films were 5, 10, 50, 100 and 500, respectively. Since the deposition ratio was 0.2 nm/cycle, as a result, the thicknesses of the ZnO films were about 1, 2, 10, 20 and 100 nm, respectively. Then we varied the deposition temperature from 60, 110 to 190 °C. The corresponding deposition rates of ALD ZnO were 0.218, 0.2 and 0.16 nm/cycle, respectively. The thickness of ALD ZnO layer was adjusted to 10 nm by controlling the growth cycle number. Subsequently, the ZnO-coated ITO substrates were transferred into a nitrogen atmosphere glove box, and a 1,2-dicholorobenzene (DCB) solution composed of P3HT (17 mg/ml, Rieke Metals) and PCBM (17 mg/ml, Nano-C) was spun onto the coated ITOs at 800 rpm for 30 s. Then the samples were baked at 110 °C for 10 min. Finally, the MoO_3 layer (10 nm) and Ag anode (100 nm) were sequentially deposited onto the active layer by thermal evaporation. The area of device was 4.5 mm^2.

The atomic force microscopy (AFM, Veeco DI Innova) was employed to characterize the morphology of ZnO film. X-ray diffraction (XRD, Bruker D8-Advance) were used to evaluate the crystal structure of the films. The thickness of ALD ZnO layer was measured by spectroscope ellipsometry (SE, HORIBA-UVISEL). The X-ray photoelectron spectroscopy (XPS) and ultraviolet photoelectron spectroscopy (UPS) were performed on Thermo ESCALAB 250 by using Al Ka X-ray source and He discharge lamp (21.22 eV), respectively. The electrical properties of the ZnO films were measured by a Hall measurement system (ECOPIA HMS-300) using the Van der Pauw method. The current density–voltage (J–V) characteristics of the devices were measured with a Keithley 2400 source measurement unit using a 100 mW/cm^2 AM 1.5G solar simulator.

3 Results and discussion

We measured the optical transmittance of ITO films modified with various thicknesses of ZnO in the UV–visible wavelength range (300–800 nm), which were shown Fig. 1. According to the transmittance spectra, the sharp absorption edge of modified ITO films shifted from about 370 nm to 390 nm when the thickness of ZnO film increased, which should be attributed to the high UV absorbance property of ZnO film at wavelength below 390 nm. In the visible wavelength range, the transmittance of ITO/ZnO film was similar with the uncoated ITO (about 85 %) when the thickness of the ZnO film was less than 20 nm. When the thickness of the ZnO film increased to 100 nm, the transmittance of ITO/ZnO layer in the range of 550–800 nm decreased to about 75 %. At the same time, the transmittance at around 480 nm was higher than the bare ITO. The increased transmittance should result from the antireflection which caused by the ZnO coating on the surface of the ITO film.

Figure 2 showed the AFM images of ITO films deposited with various thicknesses of ALD ZnO. It could be seen that the ZnO/ITO film showed the similar morphology to un-coated ITO when the thicknesses of ZnO film were 1–2 nm. The particle size of the film became larger and increased from 15 nm to 50 nm when the thickness of ZnO film increased to 10 nm. Then the particle remained the same size, about 50 nm, when the thicknesses of the ZnO film changed from 10 nm to 100 nm. Although the particle size of films changed with the varied thickness, the root

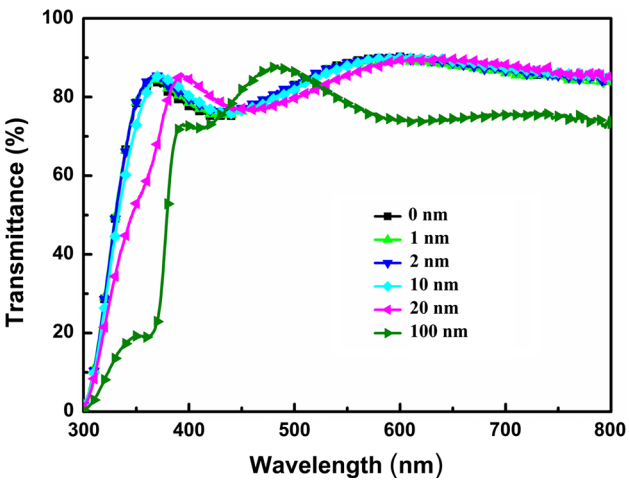

Fig. 1 The transmittance spectra of ITO (reference) and ITO/ZnO layers

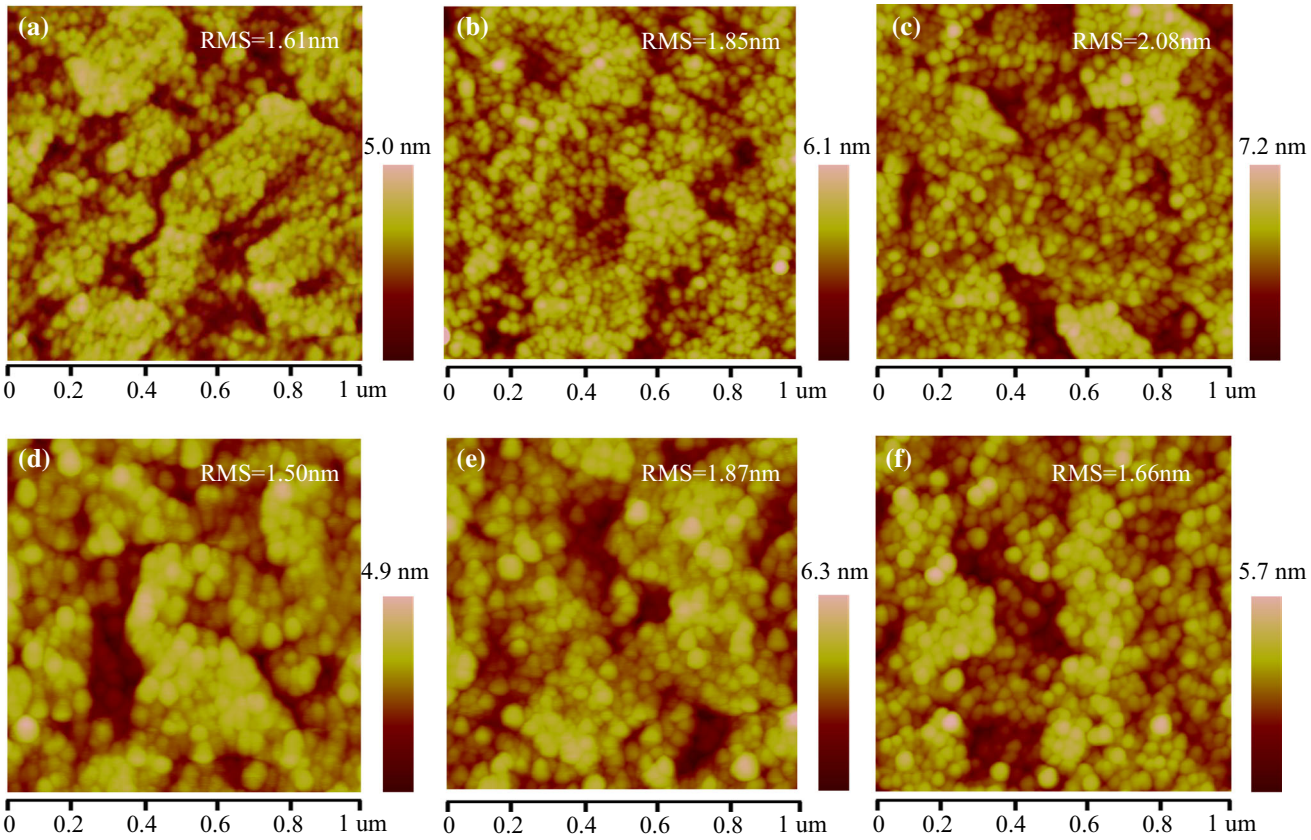

Fig. 2 The AFM images of ITO films modified with various thicknesses of ALD ZnO films (**a** 0 nm, **b** 1 nm, **c** 2 nm, **d** 10 nm, **e** 20 nm, **f** 100 nm)

mean square (RMS) values of all the ITO/ZnO layers were very small, changing from 1.50 to 2.08 nm, due to the ALD theory [27]. It was known that the RMS of ZnO films could make a direct impact on the contact between the active layer and the ZnO layer in the polymer solar cells, and thus influenced the performance of the device [29]. In our work, the low RMS value of the ALD ZnO film was beneficial for the solution-process of the active layer and the contact between the active layer and the cathode.

Figure 3(a) shows the current–voltage (*J–V*) curves of inverted devices with different thicknesses of ZnO layer. The thicknesses of ZnO films and devices parameter are summarized in Table 1. The results showed that the thickness of ALD–ZnO played an important role in the

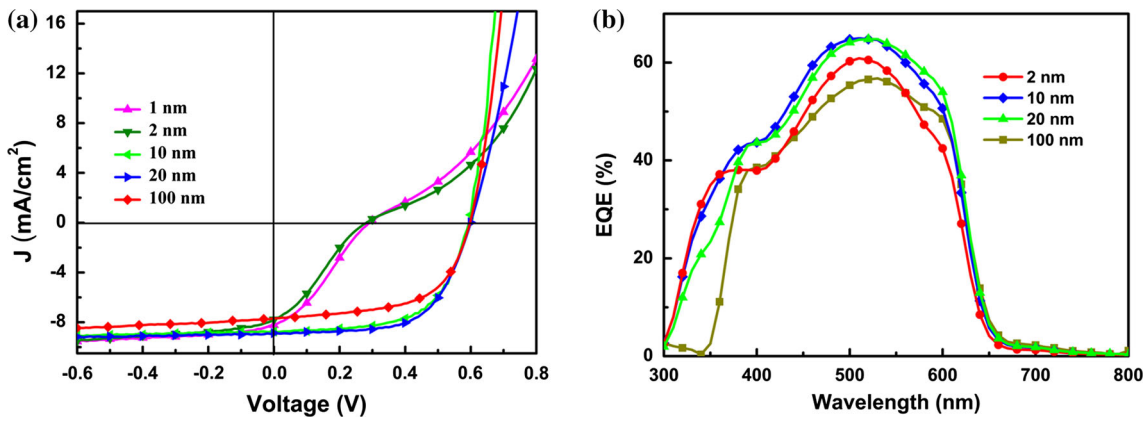

Fig. 3 *J–V* characteristics of devices with various thicknesses of ZnO films

Table 1 Photovoltaic parameters of the devices with different thicknesses of ZnO films

Deposition cycle/thickness (nm)	V_{oc} (V)	J_{sc} (mA/cm^2)	FF (%)	PCE (%)
5/∼1	0.29	8.22	30	0.72
10/∼2	0.28	7.78	28	0.61
50/∼10	0.59	8.75	62	3.20
100/∼20	0.60	8.87	62.5	3.32
500/∼100	0.60	7.69	59	2.72

performance of the device. When the thicknesses of ZnO films were about 1 and 2 nm, the device exhibited a poor performance, with the short-circuit current density (J_{sc}) of 7.78 mA/cm^2, open-circuit voltage (V_{oc}) of 0.28 V, fill factor (FF) of 0.28, and the PCE of only 0.6 %. However, with the increase of ZnO thickness, the performance of the device showed a remarkable improvement, and the device with 20 nm-thick ZnO yields the best device performance, providing the PCE of 3.32 %. These results demonstrated that enough thickness, more than 10 nm, of ZnO layer was required to enhance the efficiency of the device. Unfortunately, the further increase of ZnO thickness led to a reduction in J_{sc}. When the thickness of ZnO layer increased from 20 nm to 100 nm, the increase in the thickness resulted in a decrease in J_{sc}, which was reduced from 8.87 to 7.69 mA/cm^2; the V_{oc} remained unchanged. Figure 3(b) showed the EQE spectra of the device with different thicknesses of ZnO films. For the device with the 100-nm-thick ZnO film, the decrease in EQE over the range from 300 nm to 800 nm was observed. The decrease of EQE may partly result from the decrease of the transmittance of ITO/ZnO layer, as the decrease of the transmittance reduced the light intensity inside the active layer. In addition, ZnO film of 100 nm seems too thick which do harm to the electron extraction at cathode and result in a reduction in the device performance.

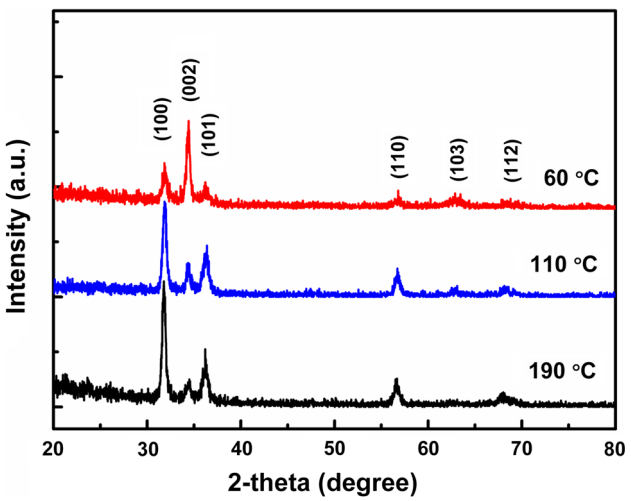

Fig. 4 XRD patterns of ZnO films grown by ALD at 60, 110 and 190 °C, respectively

Figure 4 shows the typical XRD patterns of the ZnO films deposited at different temperatures by ALD. The diffraction peaks at 31.9, 34.7 and 36.4° can be assigned to (100), (002) and (101) crystal planes of ZnO, respectively [30]. The ZnO films were polycrystalline with the hexagonal wurtzite structure, and the preferred crystal orientation of the films depended on the growth temperature. When the deposition temperature was 60 °C, the ZnO film showed strong c-axis-preferred orientations (002) because the c-axis orientation was the most densely packed and thermodynamically favorable plane in the wurtzite structure. However, the c-axis crystal growth of the film was suppressed and the preferred orientations of the ZnO films changed from *c*- to *a*-axis when the deposition temperature increased. This XRD pattern behavior was similar with the work reported by S. H. Park and S. Jeon et al., which could be explained by the characteristic of the (002) polar surface [31–33]. The ALD-grown ZnO film using DEZ and water was controlled by the reaction of metal-precursor molecules and the absorption sites of –OH groups. At higher temperature, the dissociated ethyl group could be further broken down into ethyl group fragments such as $CH_3CH_2^-$ and CH_3^- [34]. As a result, these anions adhered to the (002) polar surface of ZnO and suppressed the c-axis growth direction.

Figure 5 showed the AFM images (1 μm × 1 μm) of ALD ZnO films deposited at 60, 110 and 190 °C, respectively. The morphology of the ALD ZnO films grown at different temperatures was similar to each other. The dense and homogenous ZnO layer formed with nanoscale ZnO particles could be observed, and the grain size of the ZnO film was in the range of 40–50 nm. The root mean square (RMS) values of all the ZnO layers remain nearly the same, which were separately 1.90, 1.50 and 1.92 nm along with deposition temperature. The results showed that the deposition temperature had little influence on the morphology of the ZnO film.

Figure 6 showed high-resolution O 1 s XPS spectra of the ZnO films deposited at various deposition temperatures. The oxygen peak for all samples was found to be asymmetric with two components at around 530 eV and 531.5 eV. The lower binding energy component was

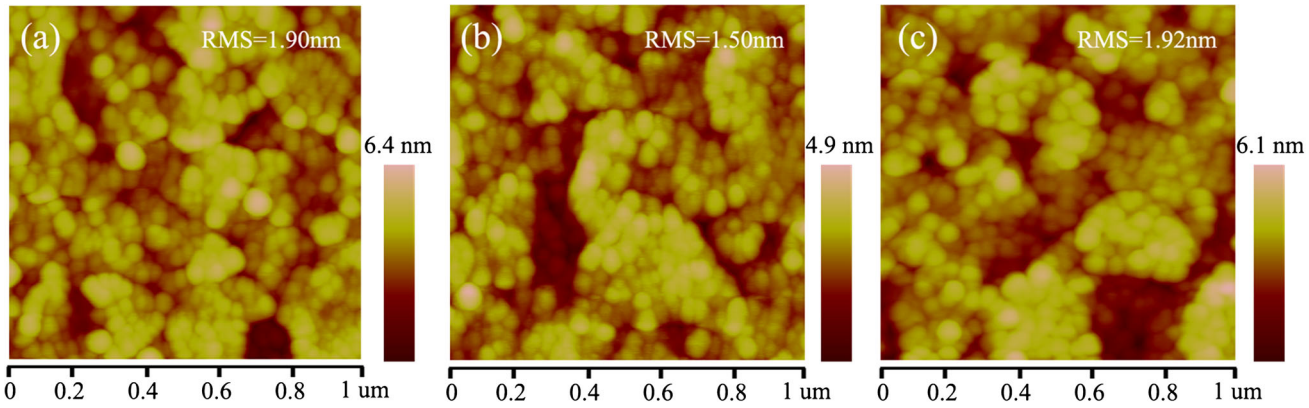

Fig. 5 The AFM images of ZnO films grown by ALD at 60, 110 and 190 °C, respectively

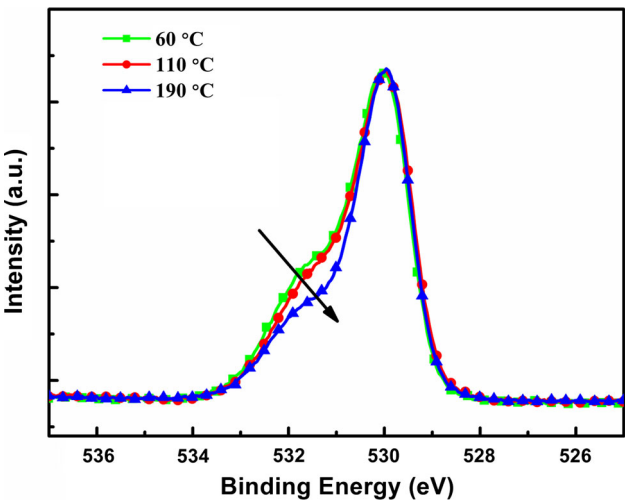

Fig. 6 Core level XPS spectra of O 1 s of ZnO films grown by ALD at 60, 110 and 190 °C, respectively

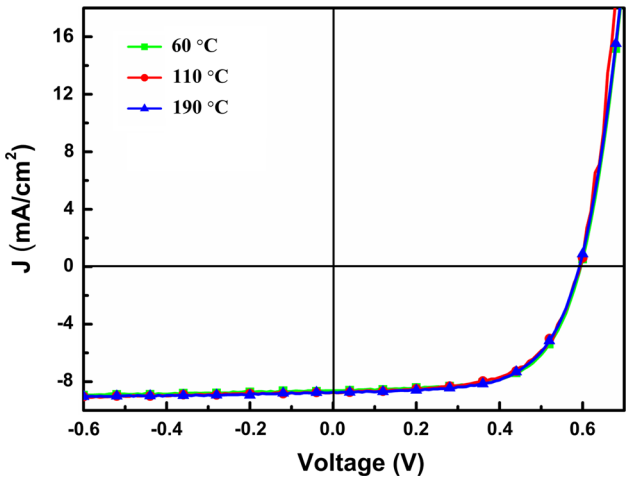

Fig. 7 *J–V* characteristics of the inverted organic solar cells with 10 nm ALD ZnO films deposited at temperature of 60, 110 and 190 °C, respectively

assigned to O^{2-} ions in the Zn–O bonding of the wurtzite structure of ZnO, whereas the higher energy component was due to –OH bonds in the ZnO films [32, 35]. The residual –OH component in ZnO was probably due to the incomplete reactions between DEZ precursors and surface –OH groups [32]. The relative area of the –OH bonding curve decreased with increasing deposition temperature as opposed to the relative area of the Zn–O bonding curve, which meant that more –OH bond was left in the film at low temperature. These residual –OH groups can behave as acceptor sites in the film matrix, and suppress the formation of oxygen vacancies [32]. To further investigate the effects of the deposition temperature on the electrical properties of ZnO films, the films were analyzed using Hall-effect measurement. All the ALD ZnO films showed n-type conductivity. And the mobility of the ZnO films deposited at 60, 110 and 190 °C were 1.2, 25, 33 cm^2/V s, respectively. The mobility of ZnO film increased with elevated deposition temperature, which should be mainly caused by the larger amount of oxygen vacancies at higher temperature.

For the application of the ZnO films as the electron transport layer in inverted solar cells, it was vital to ascertain the work functions to evaluate their electron extraction capability. For this purpose, the effect of the deposition temperature on the work function of the ZnO films was studied via the UPS measurement. The UPS spectra of the ZnO films deposited on the ITO substrates were shown in Fig. S2. The work function of ZnO film was 3.93 eV with the deposition temperature of 60 °C. When the deposition temperatures increased from 110 to 190 °C, the work function increased from 3.97 to 4.09 eV. The variation of the work function may be due to the chemical differences in the ZnO films under different deposition temperature [36]. The ALD ZnO films all reduced the work function of the ITO cathode (4.7 eV), which favored the

Table 2 Photovoltaic parameters of the devices with ZnO films deposited at different temperature

Deposition temperature (°C)	V_{oc} (V)	J_{sc} (mA/cm^2)	FF (%)	PCE (%)
60	0.59	9.0	62	3.29
110	0.59	8.86	62	3.24
190	0.59	8.8	63	3.27

Ohmic contact between LUMO of PCBM and the cathode for electron extraction. On the other hand, the slight difference in work function reduction of ITO/ZnO electrode didn't cause a notable difference in device performance, as shown in Fig. 7 and Table 2.

The *J–V* curves of the devices with ALD ZnO films as the electron transport layer is shown in Fig. 7, and the device performance parameters are summarized in Table 2. The device with ZnO film deposited at 60 °C exhibited a PCE of 3.29 % with $V_{oc} = 0.59$ V, $J_{sc} = 9$ mA/cm^2, and FF = 0.62. Similar results were obtained when the deposition temperatures of ZnO films were increased to 110 and 190 °C. This result was comparable to the device with the ZnO film fabricated by Sol–gel and sputtering [37, 38]. The efficient performance of the devices indicated that the ZnO layer could block the hole diffusion and enhanced the electron collection. We also investigated the charge collection efficiency of the devices. The J_{ph}–V_{eff} characteristics are shown in Fig. S2(a). The curves were plotted as the net photo-current density (J_{ph}) dependence on the effective applied voltage (V_{eff}), where J_{ph} was the difference between the current density under illumination (J_L) and in the dark (J_D), and $V_{appl} = V_0 - V_{appl}$ (V_0 was the compensation voltage at which $J_{ph} = 0$, V_{appl} was the applied voltage). It could be seen that J_{ph} reaches saturation for these devices at a larger verse voltage ($V_{eff} > 1$ V), which indicated that in this range nearly all the photogenerated excitons in the active layer were dissociated into free carriers and the carriers were collected without bimolecular recombination [39]. Then the charge collection efficiency could be obtained from the photocurrent density from Eq. (1).

$$P_c = J_{ph}/J_{ph,sat} \quad (1)$$

The P_c–V_{eff} curves are shown in Fig S2(b). At the short-circuit condition, the charge collection efficiencies for the devices with ZnO films deposited at different temperature were all about 96 %. And in the low effective voltage range ($V_{eff} < 0.4$ V), the charge collection efficiencies for the different devices also had the similar results. As mentioned above, the deposition temperature played an important role in the crystal quality and the electrical properties of ALD ZnO films. However, it seemed to have little influence on the charge collection ability of the ZnO films. Then ALD-grown ZnO film could be applied in the inverted solar cells as the electron transport layer in a wide range of deposition temperature from 60 to 190 °C.

4 Conclusions

In summary, more than 10 nm of ALD ZnO film was required to modify ITO for improving the photovoltaic performance of PSC. Then we prepared ZnO thin films by ALD at different temperatures and successfully utilized them as the electron transport layer to achieve efficient inverted solar cells. The obtained ZnO films all had excellent morphologies and crystal quality. The XPS and UPS analysis demonstrated that the ALD ZnO films had sufficient electronic properties to function as the electron transport layer. We also found that the performance and the charge collection efficiency of the devices were independent of the deposition temperature of ZnO films. The efficient performance was attributed to the energy level of ZnO film, which blocked the hole diffusion and was beneficial for the electron collecting. Since the deposition temperature of ZnO films could be kept in the range of 60–190 °C, this study should provide a potential approach to develop low-cost and high-efficiency plastic solar cells for practical applications.

Acknowledgments This work is supported by BIGC Project (No.23190114030, 27170115004/043) and Science and technology project of Beijing Municipal Education Commission (18190115/013).

References

1. G. Yu, J. Gao, J.C. Hummelen, F. Wudl, A.J. Heeger, Science **270**, 1789–1791 (1995)
2. P. Peumans, A. Yakimov, S.R. Forrest, J. Appl. Phys. **93**, 3693–3723 (2003)
3. F.C. Krebs, Sol. Energy Mater. Sol. Cells **93**, 394–412 (2009)
4. M. Helgesen, R. Søndergaard, F.C. Krebs, J. Mater. Chem. **20**, 36–60 (2010)
5. S.R. Cowan, N. Banerji, W.L. Leong, A.J. Heeger, Adv. Funct. Mater. **22**, 1116–1128 (2012)
6. S. Ochiai, M. Uchiyama, S. Kannappan, R. Jayaraman, P.K. Shin, Trans. Electr. Electron. Mater. **13**, 43–46 (2012)
7. M.C. Scharber, D. Muhlbacher, M. Koppe, P. Denk, C. Waldauf, A.J. Heeger, C.J. Brabec, Adv. Mater. **18**, 789–794 (2006)
8. M. Jørgensen, K. Norrman, S.A. Gevorgyan, T. Tromholt, B. Andreasen, F.C. Krebs, Adv. Mater. **24**, 580–612 (2012)

9. J.S. Kim, R.H. Friend, F. Cacialli, Appl. Phys. Lett. **74**, 3084–3086 (1999)
10. K. Kawano, R. Pacios, D. Poplavskyy, J. Nelson, D.D.C. Bradley, J.R. Durrant, Sol. Energy Mater. Sol. Cells **90**, 3520–3530 (2006)
11. M.P. de Jong, L.J. van Ijzendoorn, M.J.A. de Voigt, Appl. Phys. Lett. **77**, 2255–2257 (2000)
12. K.W. Wong, H.L. Yip, Y. Luo, K.Y. Wong, W.M. Lau, K.H. Low, H.F. Chow, Z.Q. Gao, W.L. Yeung, C.C. Chang, Appl. Phys. Lett. **80**, 2788–2790 (2002)
13. S.K. Hau, H.L. Yip, N.S. Baek, J.Y. Zou, K.O. Malley, A.K.Y. Jen, Appl. Phys. Lett. **92**, 253301–253303 (2008)
14. T.B. Yang, W.Z. Cai, D.H. Qin, E. Wang, L.F. Lan, X. Gong, J.B. Peng, Y. Cao, J. Phys. Chem. C **114**(14), 6849–6853 (2010)
15. S. Schumann, R.D. Campo, B. Illy, A.C. Cruickshank, M.A. McLachlan, M.P. Ryan, D.J. Riley, D.W. McComb, T.S. Jones, J. Mater. Chem. **21**, 2381–2386 (2011)
16. Y.H. Zhou, F.H. Li, S. Barrau, W.J. Tian, O. Inganäs, F.L. Zhang, Sol. Energy Mater. Sol. Cells **93**, 497–500 (2009)
17. Y.H. Zhou, H. Cheun, W.J. Potscavage Jr., C. Fuentes-Hernandez, S.J. Kim, B. Kippelen, J. Mater. Chem. **20**, 6189–6194 (2010)
18. F.C. Chen, J.L. Wu, K.H. Hsieh, W.C. Chen, S.W. Lee, Org. Electron. **9**, 1132–1135 (2008)
19. F.C. Chen, J.L. Wu, S.S. Yang, K.H. Hsieh, W.C. Chen, J. Appl. Phys. **103**, 103721–103725 (2008)
20. S.H. Park, A. Roy, S. Beaupre, S. Cho, N. Coates, J.S. Moon, D. Moses, M. Leclerc, K. Lee, A.J. Heeger, Nat. Photonics **3**, 297–303 (2009)
21. J.Y. Kim, S.H. Kim, H.H. Lee, K. Lee, W.L. Ma, X. Gong, A.J. Heeger, Adv. Mater. **18**, 572–576 (2006)
22. Z.Q. Liang, Q.F. Zhang, O. Wiranwetchayan, J.T. Xi, Z. Yang, K. Park, C.D. Li., G.Z. Cao. Adv. Funct. Mater. **22**, 2194–2201 (2012)
23. M.S. White, D.C. Olson, S.E. Shaheen, N. Kopidakis, D.S. Ginley, Appl. Phys. Lett. **89**, 143517–143519 (2006)
24. Z.L. Yuan, J.S. Yu, N.N. Wang, Y.D. Jiang, J. Mater. Sci.: Mater. Electron. **22**, 1730–1735 (2011)
25. T.S. Senthil, N. Muthukumarasamy, Misook. Kang, J. Mater. Sci: Mater Electron. **24**, 3963-3969 (2013)
26. N. Sekine, C.H. Chou, W.L. Kwan, Y. Yang, Org. Electron. **10**, 1473–1477 (2009)
27. J.C. Wang, W.T., Weng, M.Y. Tsai, M.K. Lee, S.F. Horng, T.P. Perng; C.C. Kei; C.C. Yu; H.F. Meng. J. Mater. Chem. **20**, 862–866 (2010)
28. R.L.Z. Hoye, D.M. Rojas, D.C. Iza, K.P. Musselman, J.L.M.M. Driscoll, Sol. Energy Mater. Sol. Cells **116**, 197–202 (2013)
29. Z.Q. Liang, Q.F. Zhang, O. Wiranwetchayan, J.T. Xi, Z. Yang, K. Park, C.D. Li, G.Z. Cao, Adv. Funct. Mater. **22**, 2194–2201 (2012)
30. X.Q. Meng, C.T. Yang, W.J. Fu, J. Wan, Mater. Lett. **83**, 179–182 (2012)
31. S.H.K. Park, C.S. Hwang, H.S. Kwack, J.H. Lee, H.Y. Chu, Electrochem. Solid-State Lett. **9**(10), G299–G301 (2006)
32. S. Jeon, S. Bang, S. Lee, S. Kwon, W. Jeong, H. Jeon, H.J. Chang, H.H. Park, J. Electrochem. Soc. **155**(10), H738–H743 (2008)
33. C.H. Ahn, S.Y. Lee, H.K. Cho, Thin Solid Films **545**, 106–110 (2013)
34. S.Y. Pung, K.L. Choy, X.H Hou, C.X. Shan, Nanotechnology. **19**, 435609(1-8) (2008)
35. R. Al-Gaashani, S. Radiman, A.R. Daud, N. Tabet, Y. Al-Douri, Ceram. Int. **39**, 2283–2292 (2013)
36. A. Sharma, D.S.E. Watkins, G. Andersson, Energy Technol. **2**, 462–468 (2014)
37. A.K.K. Kyam, X.W. Sun, C.Y. Jiang, G.Q. Lo, D.W. Zhao, D.L. Kwong, Appl. Phys. Lett. **93**, 221107 (2008)
38. H. Cheun, C. Fuentes-Hernandez, Y.H. Zhou, W.J. Potscavage Jr., S.J. Kim, J. Shim, A. Dindar, B. Kippelen, J. Phys. Chem. C **114**, 20713–20718 (2010)
39. G.K. Long, X.J. Wan, B. Kan, Z.C. Hu, X. Yang, Y. Zhang, M.T. Zhang, H.B. Wu, F. Huang, S.J. Su, Y. Cao, Y.S. Chen, ChemSusChem **7**(8), 2358–2364 (2014)